# Mapping 24 woody plant species phenology and ground forests phenology over China from 1951-2020

Mengyao Zhu[1], Junhu Dai[1,2,3], Huanjiong Wang[1], Juha M. Alatalo[4], Wei Liu[1,2], Yulong Hao[1,2], Quansheng Ge[1,2]

[1]Key Laboratory of Land Surface Pattern and Simulation, Institute of Geographic Sciences and Natural Resources Research, Chinese Academy of Sciences, Beijing, 100101, China
[2]College of Resources and Environment, University of Chinese Academy of Sciences, Beijing, 101408, China
[3]China-Pakistan Joint Research Center on Earth Sciences, CAS-HEC, Islamabad, 45320, Pakistan
[4]Environmental Science Centre, Qatar University, Doha, 2713, Qatar

*Correspondence to*: Junhu Dai (daijh@igsnrr.ac.cn); Quansheng Ge (geqs@igsnrr.ac.cn)

**Abstract.** Plant phenology refers to the cyclic plant growth events, and is one of the most important indicators of climate change. Integration of plant phenology information is of great significance for understanding the response of ecosystems to global change and simulating the material and energy balance of terrestrial ecosystems. Based on 24552 in-situ phenology observation records of 24 typical woody plants from the Chinese Phenology Observation Network (CPON), we map the species phenology (SP) and ground phenology (GP) of forests over China from 1951-2020, with a spatial resolution of 0.1° and a temporal resolution of 1 day. A model-based upscaling method was used to generate SP maps from in-situ phenology observations, and then weighted average and quantile methods were used to generate GP maps from SP maps. The validation shows that the SP maps of 24 woody plants are largely consistent with the in-situ observations, with an average error of 6.9 days in spring and 10.8 days in autumn. The GP maps of forests have good agreement with the existing Land Surface Phenology (LSP) products derived by remote sensing data, particularly in deciduous forests, with an average difference of 8.8 days in spring and 15.1 days in autumn. The dataset provides an independent and reliable phenology data source on a long-time scale of 70 years in China, and contributes to more comprehensive research on plant phenology and climate change at regional and national scales. The dataset can be accessed at https://doi.org/10.57760/sciencedb.07995 (Zhu et al., 2023).

## 1 Introduction

Plant phenology refers to plant cyclic growth and development events, which are formed by adaptation to seasonal changes in climate and environmental conditions (Lieth, 1974; Schwartz, 2003). These phenological events include critical stages such as budburst, leaf unfolding, flowering, leaf coloring, and defoliation. As a highly sensitive biological indicator of climate change (Fu et al., 2015; Richardson et al., 2013), plant phenology is not only important for comprehending ecosystem responses to global change (Menzel et al., 2020), but also a significant factor in simulating material and energy balance of terrestrial ecosystems (Keenan et al., 2014). To be helpful for biological monitoring and predictions, long-term,

dependable plant phenology data on a global scale are greatly desired by related scientific research personnel. Presently, such data can be procured from diverse sources (Piao et al., 2019; Tang et al., 2016), including manual in-situ observations (Templ et al., 2018), satellite remote sensing (Bolton et al., 2020; Dixon et al., 2021), and tower-based digital cameras (Richardson et al., 2018), etc. Nevertheless, integrating large-scale and long-term plant phenology information continues to pose a formidable challenge, owing to the substantial gaps in spatial and temporal scales between different data sources (Fisher et al., 2006; Park et al., 2021).

The practice of conducting manual, in-situ observations for species phenology (SP) boasts a rich history spanning several centuries (Aono and Kazui, 2008), yielding precise phenological information for the individual plant species (Polgar and Primack, 2011). In 1963, the Chinese Academy of Sciences inaugurated the Chinese Phenology Observation Network (CPON), a standardized, nationwide network employing a multitude of professional observers and incorporating extensive ground-based observations. To date, CPON has amassed over 1.2 million phenology records pertaining to more than 900 plant species across over 150 sites throughout China (Fig. 1), cementing its dominant status as a data center for phenological research in China. These phenology records have been contributed to examining the spatiotemporal patterns of plant phenological shifts (Dai et al., 2014; Ge et al., 2015), the environmental determinants influencing plant phenology (Dai et al., 2013; Wang et al., 2020), as well as the development of phenology models in China (Tao et al., 2018). Nonetheless, the spatial coverage of in-situ phenology data remains sporadic and restricted on regional and global scales (Donnelly et al., 2022), with noticeable gaps appearing in longer time scales. The progression of species-level phenology modeling presents an opportunity to address these limitations (Fu et al., 2020; Hufkens et al., 2018). In the absence of actual observed phenology data, phenology models can be employed to generate large-scale predictions, thereby interpolating the missing data in both space and time (Cleland et al., 2007; Wang et al., 2012). For instance, the Extended Spring Indices (SI-x) model has been successfully applied to create gridded maps illustrating the first leaf and first bloom events for three woody plants at a resolution ranging from 1° to 1 km across the contiguous United States (Ault et al., 2015; Izquierdo-Verdiguier et al., 2018). Similarly, this model-based approach can be adapted to model and map the SP data throughout China. This would enable the integration and synthesis of CPON's long-term phenology observations at regional and national scales within the country.

In contrast to manual in-situ observations, satellite remote sensing facilitates the monitoring and mapping of land surface phenology (LSP) on a more expansive scale. It provides more comprehensive LSP information at the landscape level (Studer et al., 2007). Over the past four decades, remote sensing technology has witnessed considerable advancements, significantly improving the spatial and temporal resolution (Misra et al., 2020; Dronova and Taddeo, 2022). At present, a multitude of LSP products derived from vegetation indices (e.g., NDVI and EVI) procured from multi-source remote sensing data are accessible, offering regional and global LSP data with varying spatial resolutions ranging from 10 km to 30 m (e.g., Li et al., 2019; Wu et al., 2021). The credibility of these LSP data remains largely contingent upon ground phenology (GP) validation based on in-situ observed SP data (Tian et al., 2021; Zhang et al., 2017), particularly the coordination and aggregation from individual-level phenology (i.e., SP) to landscape-level phenology (i.e., GP). Weighted average and

quantile methods have been proven effective for aggregating phenology from individual to community or landscape levels (Donnelly et al., 2022; Fitchett et al., 2015). Prior research has validated weighted average method on a site scale through field investigations and remote sensing monitoring, to aggregate GP at the community or landscape levels from in-situ SP data weighted by species abundance (Liang et al., 2011). Some recent studies have suggested that the quantile method (e.g., 30th percentile) holds greater promise than the commonly used average method on a larger scale, as evidenced in Europe and the USA (Ye et al., 2022). However, there is no previous study endeavored to employ these methods for aggregating large-scale GP from SP data in China, which may constrain the availability of ground validation evidence for LSP products and hinder comprehensive understanding of the spatio-temporal characteristics of phenological changes over the country.

In this study, we aimed to develop long-term SP and GP maps of China with a 0.1° resolution spanning 1951-2020, supplying spatially continuous grided phenology products currently absent in the country and crucial for a wider array of applications. We utilized 24,552 in-situ phenology observations of 24 representative woody plants from 122 sites over the past six decades from CPON. Three phenophases, namely the first leaf date (FLD), first flower date (FFD), and 100% leaf coloring date (LCD), were included for each species. We employed five species-level phenology models and grided meteorological data to simulate and produce SP maps, and utilized species distribution maps as masks of SP maps for each corresponding plant species. We applied weighted average and quantile methods on SP maps to aggregate and produce GP maps, which used the distribution probabilities of each species as weights. The accuracy of SP maps was assessed through cross-validation, while the reliability of GP maps was evaluated by comparing them with existing LSP products. This study introduces a novel grid phenology dataset for China, which supplements China's existing phenology data sources and provides an independent phenology data source for LSP product verification. The dataset will facilitate more comprehensive research on plant phenology and global change by better characterizing the spatiotemporal patterns of plant phenology.

## 2 Methods

### 2.1 Data acquisition and processing

#### 2.1.1 Phenology observations

The in-situ phenology observations from 1963 to 2018 were obtained from the CPON. We selected 24 species of woody plants from 17 families in China (Table 1) that are common and widespread in forest ecosystems in China (Fang et al., 2011) and well-documented in CPON. These species have been observed over 55 years in 122 sites, with a total of 24,552 records, covering a range of land cover, ecological, and climatic conditions across China (Fig. 1). Each species had at least 40 years and 13 sites of phenology data. We extracted three phenophases for each species: spring FLD, spring FFD, and autumn LCD. Three-sigma limits, which refers to data within three standard deviations from a mean, was used to set the upper and lower limits of phenology data for each species (Pukelsheim, 1994). We identified and removed outliers beyond the three-sigma lines, because they represented less than 1% of all data points on a standard normal distribution curve.

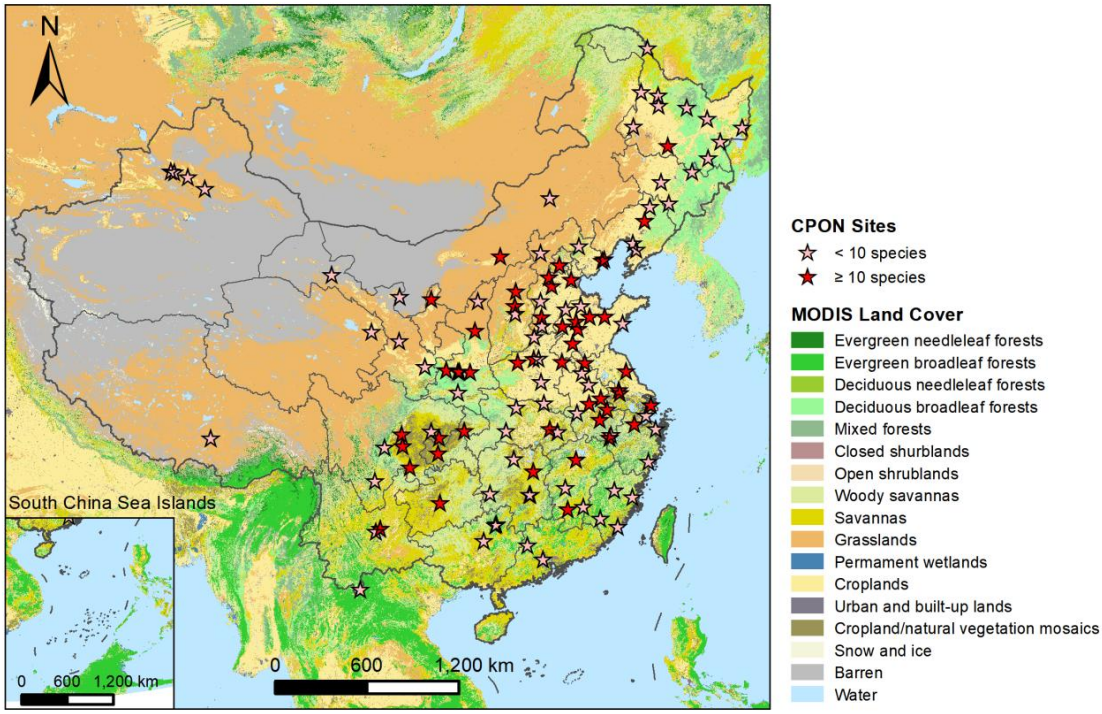


**Figure 1:** Geographic distribution of CPON sites (n = 122) included in the phenology dataset across China. Sites with less than 10 recorded species are marked with pink asterisks, while sites with more than 10 recorded species are marked with red asterisks. Note that the markings on the map of several adjacent sites may overlap each other. The background map shows the IGBP land cover type from the MODIS Land Cover product (Friedl and Sulla-Menashe, 2022).

**Table 1:** List of 24 species of woody plants from 17 families in China. Number of records represents the total number of three phenophases (FLD, FFD and LCD) of all sites and all years for each species.

| No. | Species | Family | Life form | Number of sites | Number of years | Number of records |
|---|---|---|---|---|---|---|
| 1 | *Ginkgo biloba* | Ginkgoaceae | Tree | 45 | 49 | 1110 |
| 2 | *Metasequoia glyptostroboides* | Cupressaceae | Tree | 37 | 47 | 860 |
| 3 | *Magnolia denudata* | Magnoliaceae | Tree | 42 | 47 | 980 |
| 4 | *Salix babylonica* | Salicaceae | Tree | 65 | 42 | 1526 |
| 5 | *Populus × canadensis* | Salicaceae | Tree | 43 | 51 | 954 |
| 6 | *Robinia pseudoacacia* | Fabaceae | Tree | 54 | 45 | 1757 |

| | | | | | | |
|---|---|---|---|---|---|---|
| 7 | *Albizia julibrissin* | Fabaceae | Tree | 36 | 47 | 984 |
| 8 | *Cercis chinensis* | Fabaceae | Shrub | 52 | 49 | 1207 |
| 9 | *Prunus armeniaca* | Rosaceae | Tree | 46 | 45 | 950 |
| 10 | *Ulmus pumila* | Ulmaceae | Tree | 60 | 44 | 1428 |
| 11 | *Morus alba* | Moraceae | Tree | 50 | 50 | 1071 |
| 12 | *Broussonetia papyrifera* | Moraceae | Tree | 41 | 43 | 1103 |
| 13 | *Quercus acutissima* | Fagaceae | Tree | 17 | 40 | 292 |
| 14 | *Pterocarya stenoptera* | Juglandaceae | Tree | 29 | 46 | 936 |
| 15 | *Juglans regia* | Juglandaceae | Tree | 50 | 47 | 816 |
| 16 | *Betula platyphylla* | Betulaceae | Tree | 13 | 43 | 369 |
| 17 | *Acer pictum* subsp. *mono* | Sapindaceae | Tree | 18 | 46 | 492 |
| 18 | *Ailanthus altissima* | Simaroubaceae | Tree | 34 | 47 | 873 |
| 19 | *Melia azedarach* | Meliaceae | Tree | 61 | 46 | 1410 |
| 20 | *Firmiana simplex* | Malvaceae | Tree | 57 | 48 | 1403 |
| 21 | *Hibiscus syriacus* | Malvaceae | Shrub | 58 | 47 | 1096 |
| 22 | *Fraxinus chinensis* | Oleaceae | Tree | 23 | 40 | 505 |
| 23 | *Syringa oblata* | Oleaceae | Shrub | 50 | 51 | 1163 |
| 24 | *Paulownia fortunei* | Paulowniaceae | Tree | 49 | 48 | 1267 |
| Total | | - | - | 122 | 55 | 24552 |

105

106 **2.1.2 Climate data**

107 The daily mean temperature (T) from 1950-2020 were obtained from two sources: (1) Site T was extracted from climate
108 observations in the China Meteorological Data Service Center (CMDSC, https://data.cma.cn/) and used to parameterize the
109 phenology models. (2) Grid T was extracted from ERA5-Land climate reanalysis data (Muñoz Sabater, 2019; Muñoz-
110 Sabater et al., 2021) from the Copernicus Climate Change Service (C3S, https://cds.climate.copernicus.eu/) and used for
111 phenology simulation and upscaling at a spatial resolution of 0.1° (about 10 km). Hourly grid T was averaged across four
112 phases (4:00, 10:00, 16:00, 22:00) to derive the daily grid T.

113 The current bioclimatic (BIOCLIM+) variables were obtained from Climatologies at High Resolution for the Earth
114 Land Surface Areas (CHELSA, https://chelsa-climate.org/) to determine the species distribution (Brun et al., 2022a, b). The

BIOCLIM+ variables indicate the average ecological and climatic conditions during 1981-2010, with a high resolution of 0.0083°. We extracted the traditional 19 bioclimatic layers (Bio1-Bio19) and the complementary 50 bioclimatic layers in China. We calculated the correlation between every two layers to reduce the impact of autocorrelation among these bioclimatic layers, and then excluded the layers with a correlation coefficient greater than 0.8 with the previous layers. As a result, 12 bioclimatic layers were retained as the environmental data inputs for the species distribution models (Table S1). These layers were resampled to 0.1° to match the resolution of the grid T data.

### 2.1.3 Forest and species distribution data

The forest distribution map of China was derived from the dataset of "Annual Dynamics of Global Land Cover and its Long-term Changes from 1982 to 2015" (Liu et al., 2020). Each year's land cover (LC) layers were reclassified as forest and non-forest, and then the number of years of forest cover was obtained by adding all layers. Pixels with at least one year of forest cover were identified as forest distribution areas. The forest types were identified from the most commonly used International Geosphere-Biosphere Program (IGBP) classification from MODIS Land Cover Type (MCD12C1) Version 6.1 data product (Friedl and Sulla-Menashe, 2022). We merged evergreen needleleaf forest (class 1) and evergreen broadleaf forest (class 2) into evergreen forest, and deciduous needleleaf forest (class 3) and deciduous broadleaf forest (class 4) into deciduous forest. Mixed forest (class 5) was also included in the forest type. The forest distribution map and forest type map were resampled from 0.05° to 0.1° by the majority method to match the resolution of the grid T data.

The county-level species distribution maps were obtained from the updated Database of China's Woody Plants (Fang et al., 2011). The distribution maps in this database were compiled from all national, provincial, and regional floras and inventory reports in China published before 2009, which are considered authoritative (Cai et al., 2021). We then obtained a total of 4371 occurrence records for 24 woody plant species from the Global Biodiversity Information Facility (GBIF, 2022; https://www.gbif.org/), and used them as the occurrence data inputs for the species distribution models . The occurrence records were filtered by including the coordinate locations with uncertainty less than 2000 meters, and cleaned by removing duplicate records (Table S2).

## 2.2 Generating species phenology maps using a model-based upscaling method

The generation of species phenology maps involves two major processes: (1) Generating species potential phenology maps, and (2) Generating species distribution maps. The final SP maps were obtained by spatially intersecting these two maps. The workflow for the processes is shown in Fig. 2.

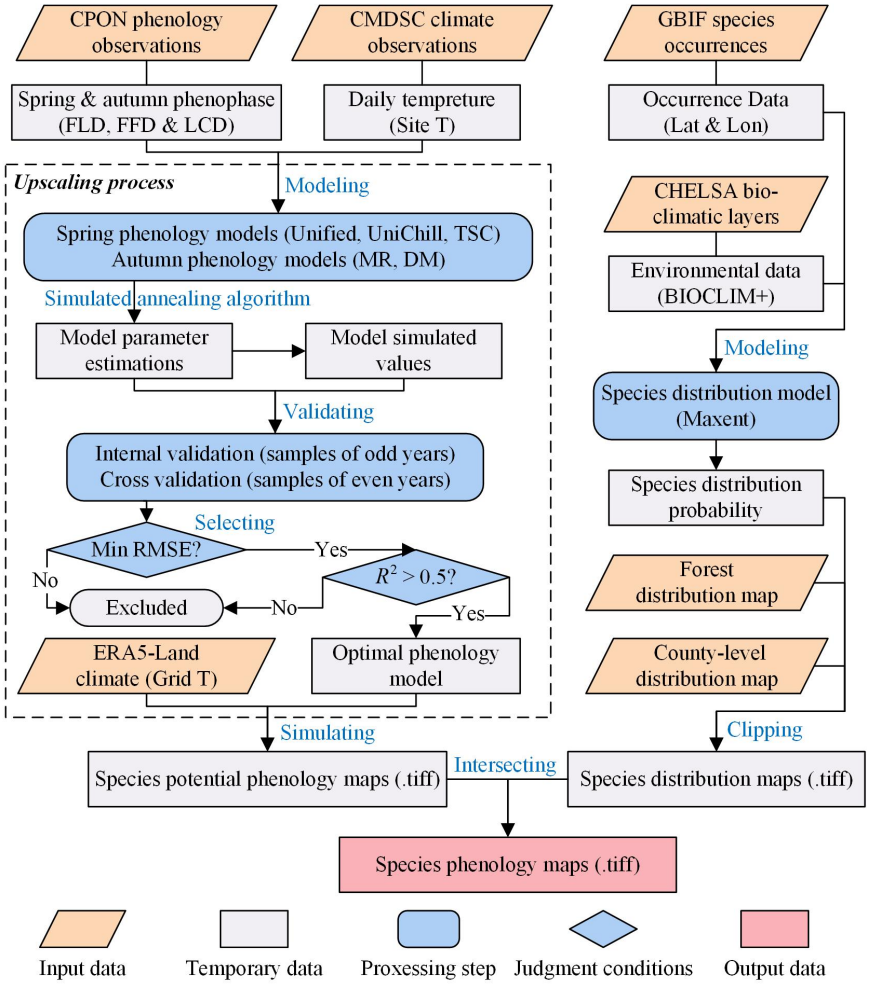


**Figure 2:** The workflow of generating SP maps using a model-based upscaling method, which involves two major processes: (1) Generating species potential phenology maps, and (2) Generating species distribution maps. The words in blue color represent the key processes of data generation. ".tiff" indicates the GeoTIFF format of the grid phenology or distribution maps.

### 2.2.1 Species potential phenology maps

In the first process, we used a model-based upscaling method to convert in-situ phenology observations into grid phenology maps. Phenology models were built using the phenophases (i.e., FLD, FFD, LCD) from CPON phenology observations and the corresponding site T from CMDSC climate observations. For each species, we built three spring phenology models: the Unichill, Unified (Chuine, 2000) and temporal-spatial coupling (TSC) models (Ge et al., 2014), and two autumn phenology models: the multiple regression (MR) (Estrella and Menzel, 2006) and temperature-photoperiod (TP)

models (Delpierre et al., 2009). The details of the model formulae are described in Appendix S1. For each model, samples from odd years were used for phenology modeling, and samples from even years were reserved for cross validation on the model. All model parameters were estimated using the simulated annealing algorithm (Chuine et al., 1998).

For model validation, the models' root mean square error (RMSE) and goodness of fit ($R^2$) were calculated between the model simulated values and original values. Internal validation was conducted on samples from odd years to evaluate the fitting effect of the model, and cross validation was conducted on samples from even years to evaluate the simulation and extrapolation effect of the model. The optimal phenology model for each species was selected based on the smallest RMSE in cross validation and $R^2$ greater than 0.5 (0.3 for LCD) in both validations. If no model met these conditions, the species was excluded when generating SP maps or GP maps.

For simulating SP maps, daily grid T data from ERA5-Land climate reanalysis were input into the optimal phenology model and simulated pixel by pixel. This way, the phenology observations from individual sites were interpolated and upscaled into a grid phenology map based on the phenology models (Chuine et al., 2000). However, as long as there was grid T data, simulated species phenology could be obtained, even if there was no species distribution. Therefore, we named it as species potential phenology map to avoid taking simulated values as true values in areas without species distribution.

### 2.1.2 Species distribution maps

In the second process, we simulated the species distribution maps using both species distribution models and county-level species distribution data. Species distribution models were built for each species using Maximum Entropy Species Distribution Modelling (Maxent; Phillips et al., 2006) version.3.4.4. Maxent estimates the range of a species by finding the species distribution of maximum entropy (i.e., closest to the uniform), which is widely adopted in species distribution modeling (Phillips et al., 2006). It expresses a probability distribution where each grid cell has a predicted probability of presence for the species. To build the Maxent model, species location records from the GBIF database were used as occurrence data input, and the 12 bioclimatic layers from BIOCLIM+ were used as the environmental data input. In the model parameter settings, linear and quadratic feature types were used and 5-fold cross validation was used as the replicated run type.

For model validation, the receiver operating characteristic (ROC) curve analysis method was used to test the accuracy of the Maxent prediction model. The area under the ROC curve, known as the AUC value, is usually used as an indicator of the prediction accuracy of the model (Fielding and Bell, 1997). The closer the AUC value is to 1.0, the more accurate the prediction result of the model is. The average test AUC for different species was 0.845, with a standard deviation of 0.043 (Table S2).

## 2.3 Generating ground phenology maps using weighted average and weighted quantile methods

We used four methods to aggregate from individual-level SP maps to landscape-level GP maps: (1) weighted average (mean); (2) weighted median (pct50); (3) weighted 20th percentile (pct20) for spring phenology or weighted 80th percentile

(pct80) for autumn phenology; (4) weighted 10th percentile (pct10) for spring phenology or weighted 90th percentile (pct90) for autumn phenology. Previous studies typically used species abundance as aggregation weights at the local scale, but it is difficult to obtain such data at the regional scale. Therefore, we used species distribution probability instead of species abundance as aggregation weight for each species. This assumption is based on a positive correlation between species distribution and abundance (Brown, 1984), demonstrating that species tend to be most abundant at the center of their geographic range (Sagarin and Gaines, 2002). The aggregation methods of GP in this study (e.g., pct50, pct20\80 and pct10\90) are comparable and similar to the extraction methods of LSP from remote sensing data (e.g., midpoint, dynamic threshold and maximum curvature). The workflow is shown in Fig. 3.

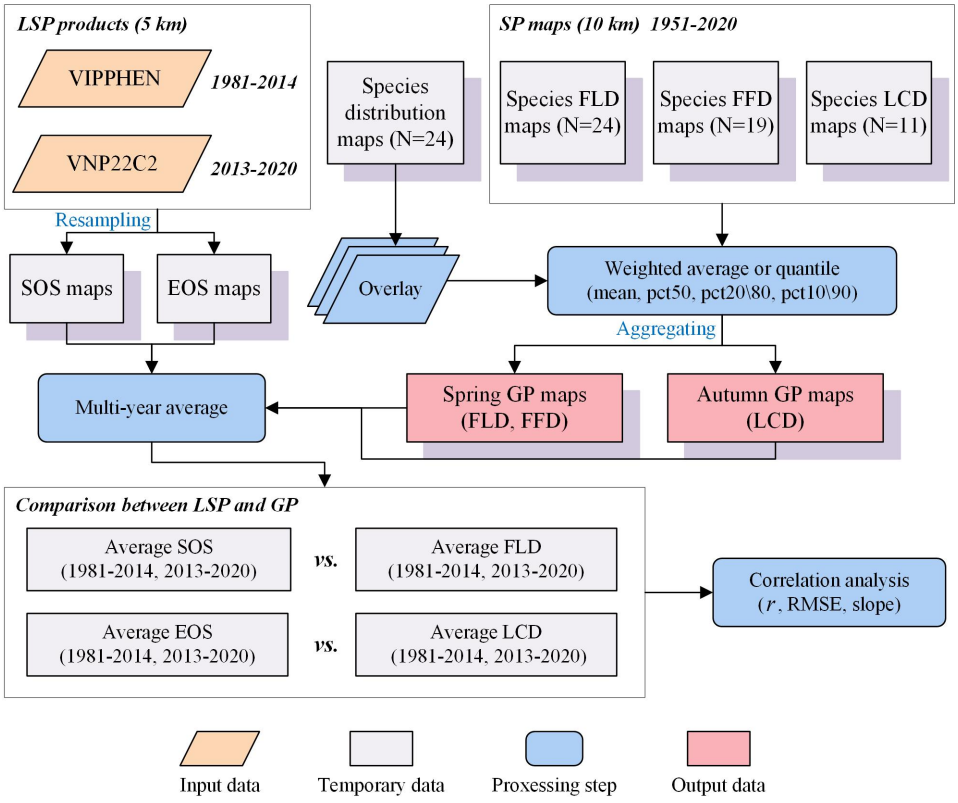


**Figure 3:** The workflow of generating GP maps from SP maps, and comparing GP maps with two LSP products. The words in blue color represent the key processes of data generation.

For $n$ species, the phenophases ($Y$) were first sorted from small to large. The SP of each species is $y_i$ ($i = 1, 2, \ldots, n$), and the distribution probability of each species is $p_i$ ($i = 1, 2, \ldots, n$). Then, the aggregated GP ($Y_{mean}$ and $Y_{pct}$ ($x\%$)) was calculated according to the following formulas:

$$\omega_i = \frac{p_i}{\sum_{i=1}^{n} p_i} \quad (1)$$

$$W_j = \sum_{i=1}^{j} \omega_i, j = 1,2,\ldots,n \quad (2)$$

$$Y_{mean} = \sum_{i=1}^{n} \omega_i \times y_i \quad (3)$$

$$Y_{pct} = \begin{cases} y_1, if\ W_1 > x \\ (y_j - y_{j-1}) \times \frac{x - W_{j-1}}{\omega_j}, if\ W_j > x, W_{j-1} < x \\ y_n, if\ W_{n-1} < x \end{cases} \quad (4)$$

Where $\omega_i$ is the weight of each species, $W_j$ is the cumulative weight from the first to the $j$ species, $x\%$ is the percentile tag which takes values from 10%, 20%, 50%, 80% and 90%. These formulas were used to calculate the aggregated GP maps by combining the species phenology maps with the species distribution maps and weighting them by the species distribution probability.

Finally, to assess data quality, the aggregated GP maps in this study were compared with two LSP products extracted from remote sensing in previous studies: (1) VIPPHEN_NDVI product (1981-2014), which used midpoint method to extract the start of season (SOS) and the end of season (EOS) from the AVHRR data (Didan and Barreto, 2016); (2) VNP22C2 product (2013-2020), which used maximum curvature method to extract SOS and EOS from the MODIS data (Zhang et al., 2020). Both LSP products were resampled from 5 km to 0.1° by the average method to match the spatial resolution of GP maps. The LSP and GP maps were averaged in two segments (1981-2014 and 2013-2020), and the correlation analysis was conducted between FLD and SOS in spring and between LCD and EOS in autumn. Pearson correlation coefficient (*r*), RMSE, and linear regression slope were used to evaluate the consistency between GP and LSP.

## 3 Results and discussion

The dataset includes two types of phenology maps over China: (1) Yearly SP maps generated by the model-based upscaling method for 24 woody plants; (2) Yearly GP maps generated by four aggregation methods, along with the corresponding quality assurance (QA) maps. The phenology maps provide spring FLD, FFD, and autumn LCD of woody plants and forests over China from 1951 to 2020, with a spatial resolution of 0.1° and a temporal resolution of 1 day. Each map is stored in a 16-bit signed integer file in GeoTIFF format, which contains a two-dimension raster (641 row × 361 column). The unit of phenology data is the Julian Day of year (DOY), which represents the actual number of days from January 1st to the date of phenology occurrence. The valid values range from DOY 1 to 366, and the null values equal to -1.

### 3.1 Simulation and validation of species phenology maps

The SP maps of FLD (24 species), FFD (19 species), and LCD (12 species) were simulated using the optimal phenology models, and then masked by the species distribution maps. Here, we present the results of simulated SP maps of four typical woody species (Fig. 4), including ginkgo (*Ginkgo biloba*), willow (*Salix babylonica*), elm (*Ulmus pumila*), and lilac (*Syringa oblata*). These maps showed that the phenophases of different species have a consistent spatial pattern of variation along latitude. Specifically, spring FLD and FFD of these species were significantly later with increasing latitude, while autumn LCD was significantly earlier with increasing latitude. Despite similar spatial patterns, the phenophases of different species show distinct temporal differences at the same latitude; for example, at lower latitudes, elm has significantly earlier spring FFD and later autumn LCD than other species. Phenophases of some species were not simulated because the $R^2$ of their optimal models was too small, e.g., $R^2 < 0.5$ for spring FFD, and $R^2 < 0.3$ for autumn LCD.

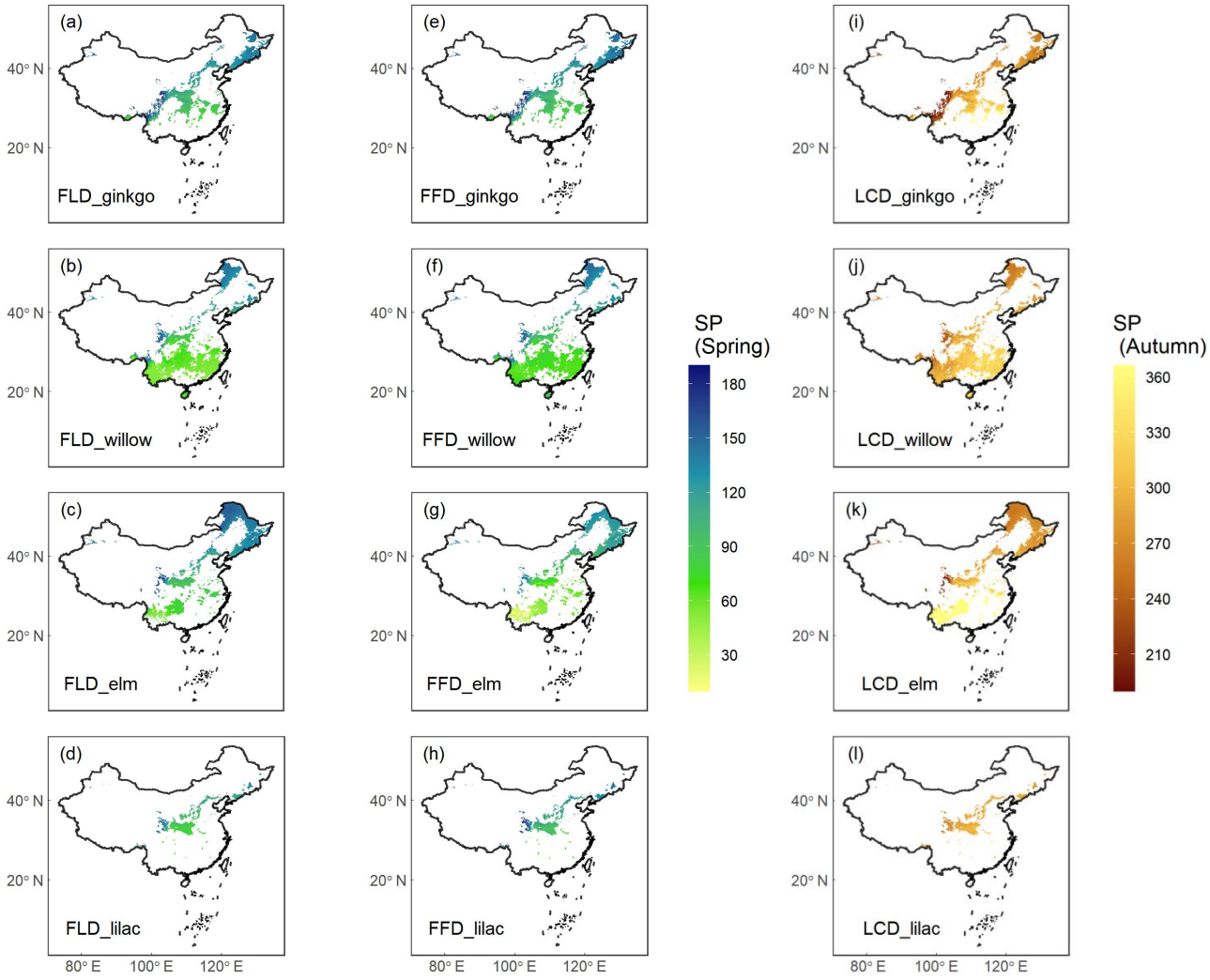


**Figure 4:** Species phenology (SP) maps of four typical woody species averaged from 1951 to 2020. Columns 1-2 show the spring phenophases (FLD and FFD), and Column 3 shows the autumn phenophase (LCD). Each row represents a species from ginkgo (*Ginkgo biloba*), willow (*Salix babylonica*), elm (*Ulmus pumila*), and lilac (*Syringa oblata*). The unit of phenology data is the Julian Day of year (DOY) from January 1st.

**Table 2:** The optimal phenology models and cross-validation results of 24 species. RMSE represents the root mean square error between the model simulated values and original values. $R^2$ represents goodness of fit of the optimal phenology model.

| No. | Species | FLD | | | FFD | | | LCD | | |
|---|---|---|---|---|---|---|---|---|---|---|
| | | Optimal model | RMSE | $R^2$ | Optimal model | RMSE | $R^2$ | Optimal model | RMSE | $R^2$ |

| | | | | | | | | | | |
|---|---|---|---|---|---|---|---|---|---|---|
| 1 | *Ginkgo biloba* | TSC | 7.30 | 0.669 | TSC | 7.53 | 0.553 | DM | 12.54 | 0.401 |
| 2 | *Metasequoia glyptostroboides* | TSC | 6.10 | 0.687 | Unified | 9.59 | 0.126 | DM | 9.99 | 0.295 |
| 3 | *Magnolia denudata* | UniChill | 6.47 | 0.781 | TSC | 7.33 | 0.576 | DM | 9.31 | 0.284 |
| 4 | *Salix babylonica* | TSC | 8.97 | 0.854 | TSC | 9.40 | 0.787 | MR | 18.23 | 0.380 |
| 5 | *Populus × canadensis* | UniChill | 5.94 | 0.808 | UniChill | 6.14 | 0.728 | MR | 9.45 | 0.139 |
| 6 | *Robinia pseudoacacia* | TSC | 5.47 | 0.863 | TSC | 6.18 | 0.785 | DM | 11.74 | 0.297 |
| 7 | *Albizia julibrissin* | UniChill | 7.48 | 0.500 | Unified | 8.23 | 0.376 | MR | 9.18 | 0.567 |
| 8 | *Cercis chinensis* | TSC | 7.90 | 0.723 | UniChill | 7.39 | 0.751 | DM | 9.09 | 0.175 |
| 9 | *Prunus armeniaca* | TSC | 6.05 | 0.865 | UniChill | 4.78 | 0.929 | MR | 14.52 | 0.191 |
| 10 | *Ulmus pumila* | UniChill | 5.09 | 0.901 | UniChill | 8.38 | 0.862 | DM | 11.16 | 0.654 |
| 11 | *Morus alba* | TSC | 6.70 | 0.905 | UniChill | 7.99 | 0.860 | DM | 9.04 | 0.175 |
| 12 | *Broussonetia papyrifera* | UniChill | 7.60 | 0.804 | TSC | 6.18 | 0.821 | DM | 9.97 | 0.615 |
| 13 | *Quercus acutissima* | UniChill | 6.73 | 0.931 | UniChill | 5.12 | 0.950 | MR | 14.35 | 0.765 |
| 14 | *Pterocarya stenoptera* | UniChill | 7.52 | 0.804 | UniChill | 7.89 | 0.710 | MR | 11.57 | 0.415 |
| 15 | *Juglans regia* | TSC | 6.04 | 0.739 | UniChill | 8.54 | 0.595 | DM | 8.41 | 0.141 |
| 16 | *Betula platyphylla* | UniChill | 3.80 | 0.915 | UniChill | 3.70 | 0.906 | DM | 8.27 | 0.655 |
| 17 | *Acer pictum* subsp. *mono* | TSC | 2.29 | 0.894 | TSC | 3.78 | 0.814 | DM | 4.71 | 0.670 |
| 18 | *Ailanthus altissima* | UniChill | 5.22 | 0.867 | UniChill | 8.34 | 0.664 | DM | 10.39 | 0.066 |
| 19 | *Melia azedarach* | TSC | 6.81 | 0.828 | TSC | 6.70 | 0.851 | MR | 10.19 | 0.135 |
| 20 | *Firmiana simplex* | UniChill | 6.02 | 0.694 | Unified | 8.10 | 0.314 | DM | 12.30 | 0.190 |
| 21 | *Hibiscus syriacus* | TSC | 9.66 | 0.666 | Unified | 13.38 | 0.331 | DM | 12.76 | 0.464 |
| 22 | *Fraxinus chinensis* | TSC | 6.25 | 0.852 | Unified | 12.35 | 0.319 | MR | 9.76 | 0.533 |
| 23 | *Syringa oblata* | UniChill | 7.01 | 0.864 | UniChill | 5.11 | 0.920 | MR | 12.36 | 0.475 |
| 24 | *Paulownia fortunei* | UniChill | 4.63 | 0.762 | UniChill | 7.02 | 0.693 | MR | 10.01 | 0.250 |

The simulation effects of species phenology maps were evaluated by cross-validation on the optimal phenology models (Table 2). The results showed that the simulation effects of spring phenology were significantly better than that of autumn phenology (Fig. 5). Specifically, the RMSE of the optimal model of FLD (6.38 days) and FFD (7.46 days) in spring were

significantly smaller than that of LCD (10.80 days) in autumn. And the $R^2$ of the optimal model of FLD (0.799) and FFD (0.676) in spring were significantly greater than that of LCD (0.372) in autumn. However, there was no significant difference between spring FLD and FFD simulation effects. Among the optimal spring phenology models, the FFD simulation effects of UniChill and TSC models were significantly better than Unified model.. But in autumn, the LCD simulations effects are similar for MR and TP models.

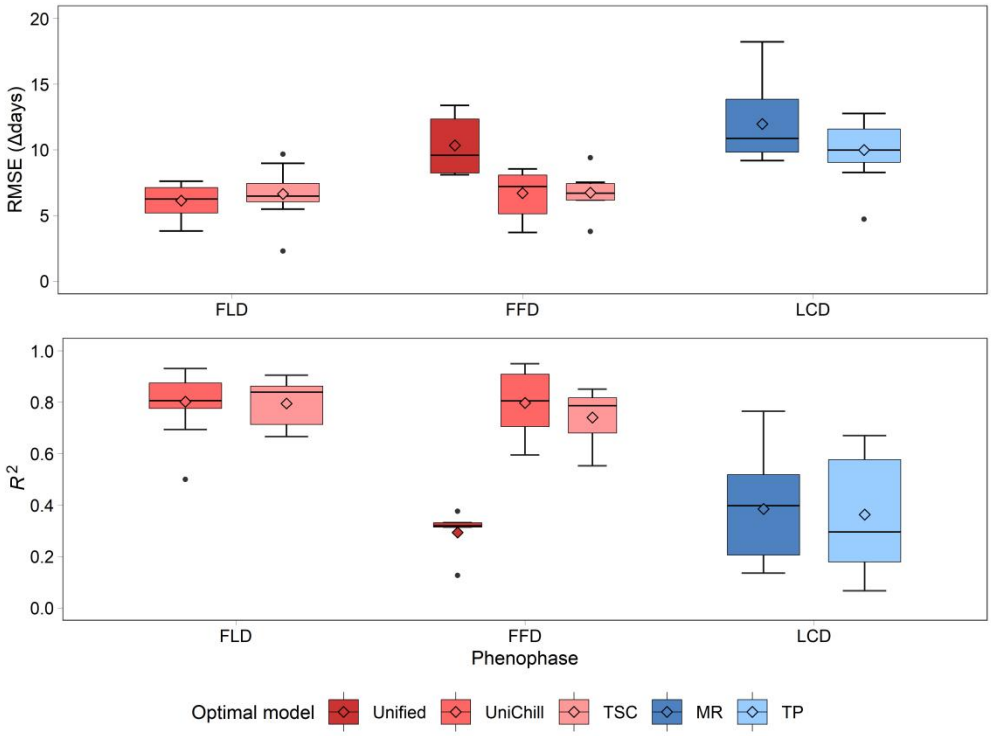


**Figure 5:** The RMSE (a) and $R^2$ (b) of cross-validation on the optimal phenology models for 24 woody species. Each model is represented by a different color, with warm colors for three spring phenology models (Unified, UniChill, TSC), and cool colors for two autumn phenology models (MR, TP). The model with the smallest RMSE was selected as the optimal model for each species. The horizontal line represents the median value, the diamond mark represents the mean value, and the dot mark represents the outlier in the boxplot.

### 3.2 Aggregation of ground phenology maps

The results of GP maps generated by four different aggregation methods (mean, pct50, pct20\80, pct10\90) showed similar spatial patterns (Fig. 6), i.e., the consistent variation along latitude or altitude. With the increase of latitude or altitude, the spring GP (FLD and FFD) became later, and the autumn GP (LCD) became earlier. For different aggregation methods, the GP maps aggregated from the mean and pct50 methods were highly consistent, with *r* being 0.992; while the

GP maps aggregated from the pct20\80 and pct10\90 methods were slightly different from the former two, with *r* being 0.968 and 0.949, and showed larger spatial variation than the former two. The high consistency between the mean and pct50 maps indicated that both the weighted mean method and weighted quantile method were robust for the aggregation of GP.

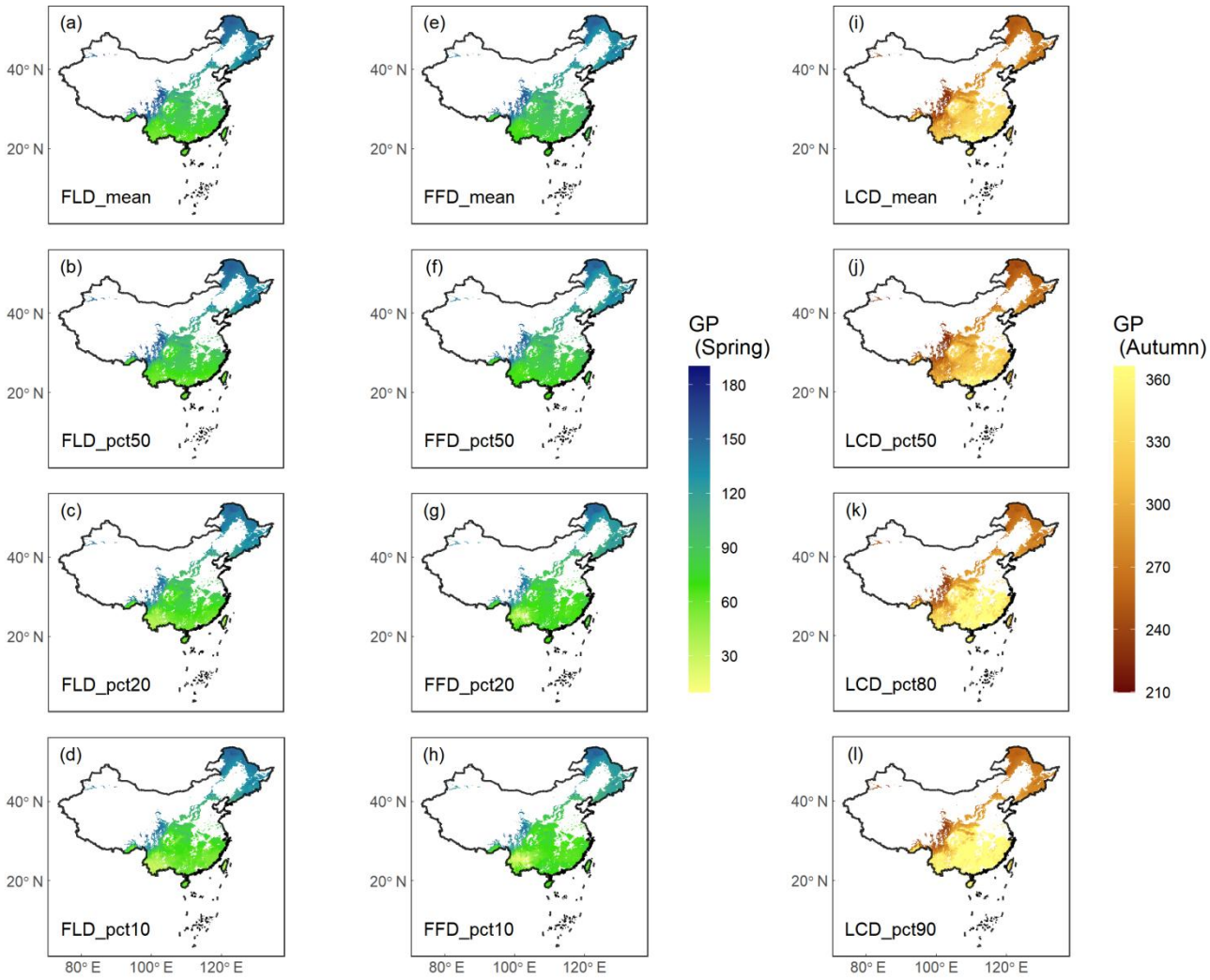


**Figure 6:** Ground phenology (GP) maps of four aggregation methods averaged from 1951 to 2020. Columns 1-2 show the spring phenophases (FLD and FFD), and Column 3 shows the autumn phenophase (LCD). Each row represents an aggregation method from weighted average (mean), weighted median (pct50), weighted 20% or 80% percentile (pct20\80), and weighted 10% or 90% percentile (pct10\90). The unit of GP is the Julian Day of year (DOY) from January 1st.

We also provided two QA maps to evaluate the reliability of the aggregation results of GP maps (Fig. S1). The first is the total distribution probability of all species, and the second is the total number of species with distribution probabilities greater than 0.1. In the QA maps, higher values mean larger total number or probability of species for the aggregation, indicating that GP maps have higher reliability in these areas. The regions with the most reliable GP aggregation results were distributed around 30° N in China. The total number of species is about 15 for FLD and FFD, and is about 6 for LCD in these regions. It should be noted that in the QA map, in areas where the total number of species is less than 5 or the total probability of species is less than 1, the aggregation results of GP may not be reliable.

### 3.3 Data quality and usability

GP and LSP were compared between FLD and SOS in spring and between LCD and EOS in autumn during two segments (1981-2014 and 2013-2020). The results showed that GP and two LSP products had similar spatial patterns in central and northern China but relatively different patterns in southern China (Fig. 7), particularly for LCD and EOS in autumn (Fig. 7e-h). This is likely due to the prevalence of deciduous forests in central and northern China (Fig. 1). In contrast, evergreen and mixed forests are found in southern China. GP in this study was generated by aggregating the phenology of 24 deciduous woody plants, which made up a large proportion of deciduous forests but a small proportion of evergreen or mixed forests. Additionally, LSP extracted from remote sensing data tends to have a larger error in evergreen and mixed forests due to the lack of obvious seasonal change and frequent cloud cover in these regions (Liu et al., 2016b). As a result, the consistency between GP and LSP was relatively poor in evergreen or mixed forests (Fig. S2), with the maximum $r$ being 0.44 in spring and 0.54 in autumn, and the minimum RMSE being 28.5 days in spring and 38.5 days in autumn (Table S2). In contrast, the consistency between GP and LSP was much better in deciduous forests, with the maximum $r$ being 0.95 in spring and 0.88 in autumn, and the minimum RMSE being 8.8 days in spring and 15.1 days in autumn, respectively.

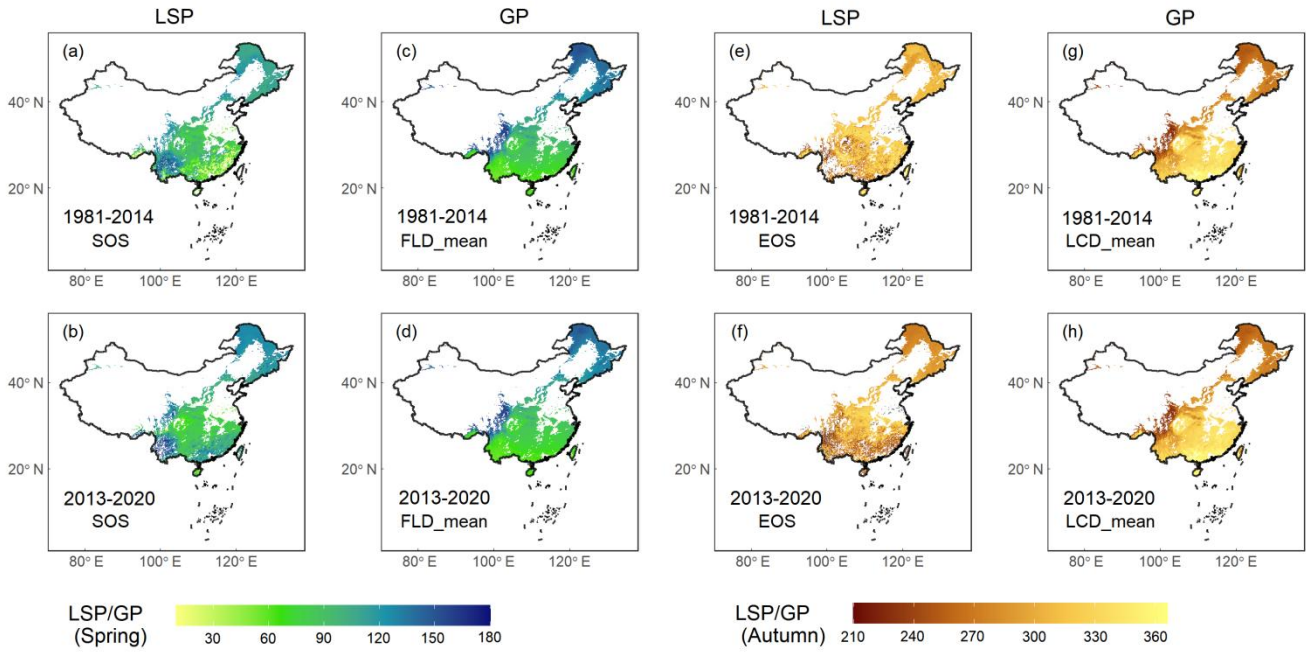


**Figure 7:** Comparison of GP maps in this study and two LSP products (VIPPHEN and VNP22C2) extracted from remote sensing in previous studies, which was made between FLD and SOS in spring and LCD and EOS in autumn. Row 1 shows the comparison between VIPPHEN product and GP map averaged in 1981-2014, and Row 2 shows the comparison between VNP22C2 product and GP map averaged in 2013-2020. (a-b) SOS from two LSP products; (c-d) FLD aggregated by mean method; (e-f) EOS from two LSP products; (g-h) LCD aggregated by mean method. The unit of GP or LSP is the Julian Day of year (DOY) from January 1st.

To further assess the quality of the data, we examined the consistency between GP and LSP specifically in deciduous forests. The results showed that GP and LSP had good consistency for both VIPPHEN and VNP22C2 products, i.e., high correlation, small difference, and good linear relationship (Fig. 8). Compared with the LSP of VIPPHEN product, the LSP of VNP22C2 product has better consistency with the GP of this study. In addition, for both products, the consistency between GP and LSP in spring (Fig. 8e, g) was significantly better than that in autumn (Fig. 8f, h). When comparing different aggregation methods (mean, pct50, pct20/80, pct10/90), there was no significant difference in *r* between GP and LSP (Fig. 8a, b). All methods produced similar *r* values, ranging from 0.76-0.78 in spring and 0.49-0.53 in autumn for the VIPPHEN product, and from 0.90-0.91 in spring and 0.79-0.84 in autumn for the VNP22C2 product. However, different methods produced significantly different RMSE values between GP and LSP (Fig. 8c, d), largely due to the differences in the average values of GP under different methods. The best aggregation methods, with the minimum RMSE, were pct10 (20.8 days) in

spring and pct90 (32.9 days) in autumn for the VIPPHEN product, and pct20 (8.8 days) in spring and pct90 (15.1 days) in autumn for the VNP22C2 product.

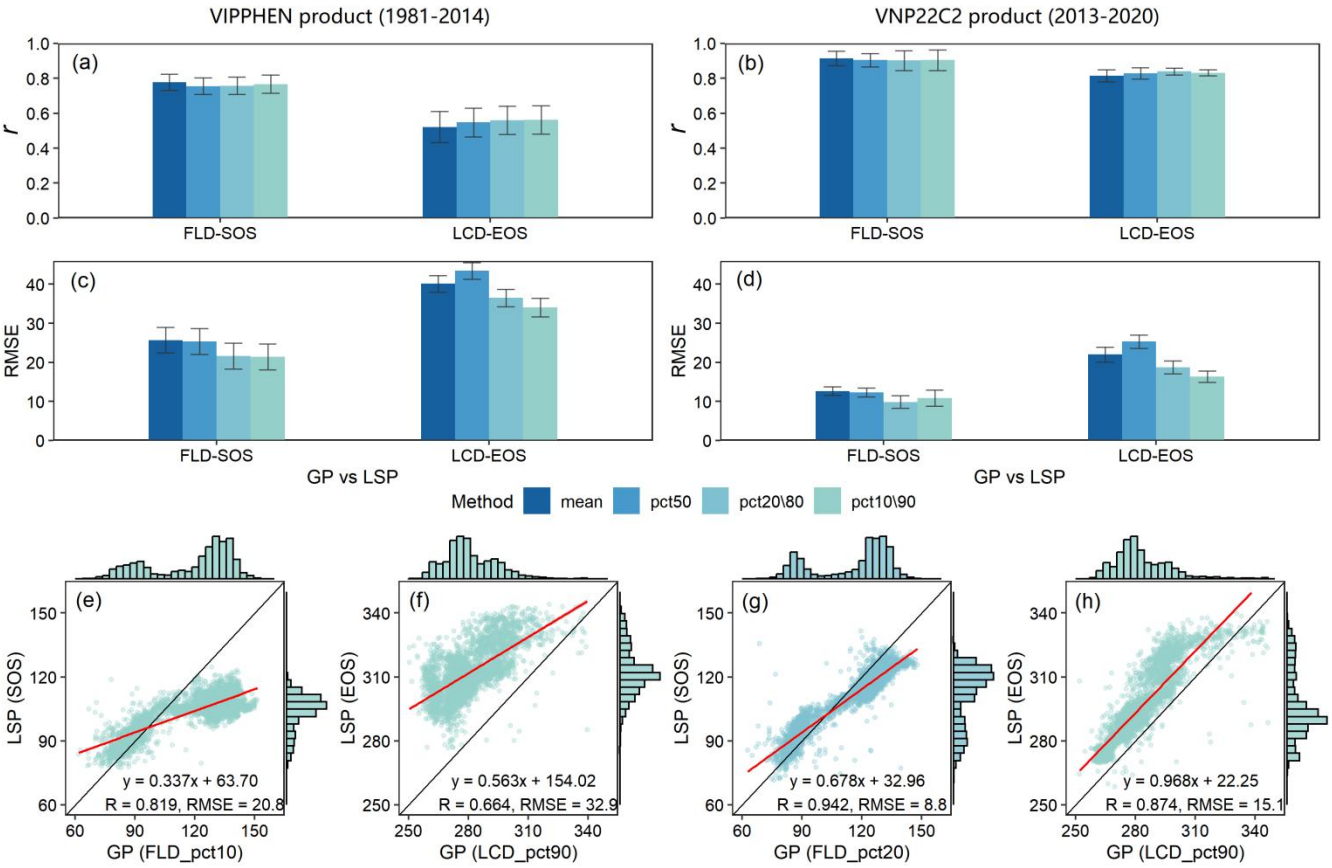


**Figure 8:** Comparison results of GP maps and two LSP products (VIPPHEN and VNP22C2) in deciduous forests, which was made between FLD and SOS in spring and LCD and EOS in autumn within the time range 1981-2014 and 2013-2020. (a-b) *r* between LSP and GP under four aggregating methods; (c-d) RMSE between LSP and GP under four aggregating methods; (e-h) Linear relationship between between LSP and GP under the best aggregating method. Each aggregating method is represented by a different color. The best aggregating method was determined by minimizing the RMSE between GP and LSP. The error bar in the bar plot represents the multi-year standard deviation. The red line in the scatter plot represents the linear regression line between GP and LSP, and all regression results were extremely significant ($p<0.001$).

It is worth noting that the aggregation method with the smallest difference between GP and LSP in this study was the 10th or 20th percentile in spring and the 90th percentile in autumn. It means that the spring green-up event detected by remote sensing is more consistent with the FLD of earlier-developing plant species (the first 10%-20%) on the ground, while the autumn dormancy event from remote sensing is more consistent with the LCD of later-senescent plant species (the last

10%) on the ground. These results reveal a potential connection between GPs and LSPs despite their different physical implications in diagnosing phenology.

In general, this dataset provides high reliability species and ground phenology simulations of forests over China for the past 70 years. It is an independent phenology data source generated by the modeling and aggregation based on ground observations. There are several considerations in data application:

(1) For SP maps, the accuracy of data was determined by RMSE and $R^2$ of cross-validation on the optimal phenology model for each species (Table 2). Additionally, the reliability of phenology data in space was affected by the number of sites available for modeling on each species (Table 1). For instance, the accuracy of *Betula platyphylla*'s FLD was very high overall (RMSE = 3.80 and $R^2$ = 0.915), but the local accuracy might be relatively poor in areas with sparse sites due to very few sites of *Betula platyphylla* in space (n = 13). In this study, the SP maps of 24 species in China were found to be largely consistent with the in-situ observations, with an average error of 6.4, 7.5 and 10.8 days for FLD, FFD and LCD, respectively. These errors were the same or smaller than those of phenology modelling in previous studies. For example, the simulation error of spring FLD and FFD was 7-9 days in central Europe (Basler, 2016) and was 12.3-12.7 days in the United States (Izquierdo-Verdiguier et al., 2018), while the simulation error of autumn LCD was 10.3-13.0 days in France (Delpierre et al., 2009) and 5.9-22.8 days in the United States (Jeong and Medvigy, 2014). Therefore, compared with other studies on the regional scale, the SP maps of China in this study were found to have relatively high accuracy.

(2) For GP maps, the reliability of data can be determined by QA maps which provide the total number or probability of species. Additionally, the reliability can also be evaluated by comparing GP data with other LSP products, with high consistency indicating good reliability. Since GP data actually provide phenology estimates of the deciduous components in the forests, it has better reliability in the deciduous forests but less reliability in evergreen or mixed forests. In this study, GP maps of forests in China were found have good consistency with the existing LSP products, particularly in deciduous forests, where the correlation coefficients of FLD and LCD were 0.91 and 0.84, respectively. The differences between GP and LSP in FLD and LCD were also found to be relatively small in deciduous forests, being 8.8 days and 15.1 days, respectively. Previous studies have shown poor consistency between single species and LSP, with correlation coefficients ranging from 0.50 to 0.51 in the United States (Peng et al., 2017) and Germany (Kowalski et al., 2020), and differences ranging from 12 to 14.5 days in the United States (Peng et al., 2017) and Canada (Delbart et al., 2015). In contrast, research comparing average or quantile values of multiple species has shown better results similar to this study. For example, the correlation coefficients between the average (or weighted average) GP and LSP were found to be 0.61 to 0.71 in Europe (Rodriguez-Galiano et al., 2015; Tian et al., 2021). The correlation coefficients between the 30th percentile GP and LSP were found to be 0.54 to 0.57 in China (Wu et al., 2016). The differences between the GP and LSP in previous studies were 10.3-12.4 days in China (Wu et al., 2016), 13.9 days in Europe, and 12.3 days in the United States (Ye et al., 2022), which was larger than the results of FLD but smaller than that of LCD in this study. Although the landscape-level GP data aggregated from species-level phenology data in this study showed good reliability, limitations in available species and different aggregation methods suggest that future comparisons between GP and LSP in other regions still need to be improved.

(3) For phenology maps in different seasons, the reliability of phenology data in spring was found to be significantly higher than that in autumn. The underlying reason is that the mechanism of autumn phenology is more complex compared to that of spring phenology (Menzel, 2002). Moreover, the driving mechanisms for the autumn phenology are complex, which poses an additional challenge (Gill et al., 2015; Wu et al., 2018). For example, temperature has large effects on the autumn phenology than the spring phenology (Fu et al., 2018). In addition to temperature, other environmental factors such as precipitation (An et al., 2020), photoperiod (Lang et al., 2019), solar radiation (Wu et al., 2021b), spring phenology (Liu et al., 2016a), and growing-season productivity (Zani et al., 2020) may also drive autumn phenology. Thus, modeling autumn phenology is more challenging compared to spring phenology (Melaas et al., 2016), resulting in poorer model performance and inferior data quality of SP or GP maps in autumn.

## 4 Data availability

The annual SP and GP maps over China can be accessed at https://doi.org/10.57760/sciencedb.07995 (Zhu et al., 2023). This dataset is licensed under a CC-BY 4.0 license. The spatial reference system of the dataset is EPSG:4326(WGS84).

## 5 Conclusions

In this study, mainly based on CPON historical phenology observations, we developed a new long-term gridded phenology dataset: SP maps of 24 woody plants and GP maps of forests over China from 1951–2020, with a spatial resolution of 0.1° and a temporal resolution of 1 day. For the generation of SP maps, we adopted a model-based upscaling method to realize the scale expansion of phenology date from in-situ to regional scales in China. For the generation of GP maps, we adopted weighted average and weighted quantile methods to realize the aggregation from species to community or landscape levels in China. Dataset quality assessment shows that the average error of SP maps is 6.9 days in spring and 10.8 days in autumn, and the minimum difference between GP maps and existing LSP products is 8.8 days in spring and 15.1 days in autumn. Compared to the previous studies (Basler, 2016; Delpierre et al., 2009; Izquierdo-Verdiguier et al., 2018; Jeong and Medvigy, 2014; Tian et al., 2021; Wu et al., 2016; Ye et al., 2022), the SP maps in this study have the same or smaller simulation error, and the GP maps in this study have good agreement with other LSP products, so the data has high accuracy and reliability. This dataset is the first phenology map of China. It can be used to investigate the spatial pattern of plant phenology more clearly along the geographic gradient (e.g., longitude, latitude, and altitude), and to reveal the temporal trends (e.g., interannual, decadal, and secular) of plant phenology across China. The dataset can also provide important data support for global change impact assessment, terrestrial ecosystem simulation, and natural resource management.

## Author contribution

QG and JD designed the study and planned the modeling. HW developed the model code. WL and YH performed the simulations. MZ processed the modeling data, performed the computations and drafted the manuscript. JD and JA critically revised the manuscript. All authors discussed and contributed to the modeling and manuscript.

## Competing interests

The authors declare that they have no conflict of interest.

## Acknowledgements

This study was jointly supported by National Key Research and Development Program of China (2018YFA0606102), National Natural Science Foundation of China (42271062), and Strategic Priority Research Program (A) of Chinese Academy of Sciences (XDA19020303; XDA26010202). Phenology data was provided by CPON. Temperature data was provided by Copernicus Climate Change Service (C3S).

## References

An, S., Chen, X., Zhang, X., Lang, W., Ren, S., and Xu, L.: Precipitation and minimum temperature are primary climatic controls of alpine grassland autumn phenology on the Qinghai-Tibet Plateau, Remote Sens., 12, 431, https://doi.org/10.3390/rs12030431, 2020.

Aono, Y. and Kazui, K.: Phenological data series of cherry tree flowering in Kyoto, Japan, and its application to reconstruction of springtime temperatures since the 9th century, Int. J. Climatol., 28, 905–914, https://doi.org/10.1002/joc.1594, 2008.

Ault, T. R., Schwartz, M. D., Zurita-Milla, R., Weltzin, J. F., and Betancourt, J. L.: Trends and natural variability of spring onset in the coterminous United States as evaluated by a new gridded dataset of spring indices, J. Clim., 28, 8363–8378, https://doi.org/10.1175/jcli-d-14-00736.1, 2015.

Basler, D.: Evaluating phenological models for the prediction of leaf-out dates in six temperate tree species across central Europe, Agric. For. Meteorol., 217, 10–21, https://doi.org/10.1016/j.agrformet.2015.11.007, 2016.

Bolton, D. K., Gray, J. M., Melaas, E. K., Moon, M., Eklundh, L., and Friedl, M. A.: Continental-scale land surface phenology from harmonized Landsat 8 and Sentinel-2 imagery, Remote Sens. Environ., 240, 111685, https://doi.org/10.1016/j.rse.2020.111685, 2020.

Brown, J. H.: On the Relationship between Abundance and Distribution of Species, Am. Nat., 124, 255–279, https://doi.org/10.1086/284267, 1984.

Brun, P., Zimmermann, N., Hari, C., Pellissier, L., and Karger, D.: CHELSA-BIOCLIM+ A novel set of global climate-related predictors at kilometre-resolution, EnviDat [data set], 10, 2022a.

Brun, P., Zimmermann, N. E., Hari, C., Pellissier, L., and Karger, D. N.: Global climate-related predictors at kilometer resolution for the past and future, Earth Syst. Sci. Data, 14, 5573–5603, https://doi.org/10.5194/essd-14-5573-2022, 2022b.

Cai, H., Lyu, L., Shrestha, N., Tang, Z., Su, X., Xu, X., Dimitrov, D., and Wang, Z.: Geographical patterns in phylogenetic diversity of Chinese woody plants and its application for conservation planning, Divers. Distrib., 27, 179–194, https://doi.org/10.1111/ddi.13180, 2021.

Chuine, I.: A unified model for budburst of trees, J. Theor. Biol., 207, 337–347, https://doi.org/10.1006/jtbi.2000.2178, 2000.

Chuine, I., Cour, P., and Rousseau, D.: Fitting models predicting dates of flowering of temperate-zone trees using simulated annealing, Plant Cell Environ., 21, 455–466, https://doi.org/10.1046/j.1365-3040.1998.00299.x, 1998.

Chuine, I., Cambon, G., and Comtois, P.: Scaling phenology from the local to the regional level: advances from species-specific phenological models, Global Change Biol., 6, 943–952, https://doi.org/10.1046/j.1365-2486.2000.00368.x, 2000.

Cleland, E. E., Chuine, I., Menzel, A., Mooney, H. A., and Schwartz, M. D.: Shifting plant phenology in response to global change, Trends Ecol. Evol., 22, 357–365, https://doi.org/10.1016/j.tree.2007.04.003, 2007.

Dai, J., Wang, H., and Ge, Q.: Multiple phenological responses to climate change among 42 plant species in Xi'an, China, Int. J. Biometeorol., 57, 749–758, https://doi.org/10.1007/s00484-012-0602-2, 2013.

Dai, J., Wang, H., and Ge, Q.: Characteristics of spring phenological changes in China over the past 50 years, Adv. Meteorol., 2014, 1–8, https://doi.org/10.1155/2014/843568, 2014.

Delbart, N., Beaubien, E., Kergoat, L., and Le Toan, T.: Comparing land surface phenology with leafing and flowering observations from the PlantWatch citizen network, Remote Sens. Environ., 160, 273–280, https://doi.org/10.1016/j.rse.2015.01.012, 2015.

Delpierre, N., Dufrêne, E., Soudani, K., Ulrich, E., Cecchini, S., Boé, J., and François, C.: Modelling interannual and spatial variability of leaf senescence for three deciduous tree species in France, Agric. For. Meteorol., 149, 938–948, https://doi.org/10.1016/j.agrformet.2008.11.014, 2009.

Didan, K. and Barreto, A.: NASA MEaSUREs Vegetation Index and Phenology (VIP) Phenology NDVI Yearly Global 0.05Deg CMG, NASA EOSDIS Land Processes DAAC, accessed on 2022-08-11, https://doi.org/10.5067/MEaSUREs/VIP/VIPPHEN_NDVI.004, 2016.

Dixon, D. J., Callow, J. N., Duncan, J. M., Setterfield, S. A., and Pauli, N.: Satellite prediction of forest flowering phenology, Remote Sens. Environ., 255, 112197, https://doi.org/10.1016/j.rse.2020.112197, 2021.

Donnelly, A., Yu, R., Jones, K., Belitz, M., Li, B., Duffy, K., Zhang, X., Wang, J., Seyednasrollah, B., Gerst, K. L., and others: Exploring discrepancies between in situ phenology and remotely derived phenometrics at NEON sites, Ecosphere, 13, e3912, https://doi.org/10.1002/ecs2.3912, 2022.

Dronova, I. and Taddeo, S.: Remote sensing of phenology: Towards the comprehensive indicators of plant community dynamics from species to regional scales, J. Ecol., 110, 1460–1484, https://doi.org/10.1111/1365-2745.13897, 2022.

Estrella, N. and Menzel, A.: Responses of leaf colouring in four deciduous tree species to climate and weather in Germany, Clim. Res., 32, 253–267, https://doi.org/10.3354/cr032253, 2006.

Fang, J., Wang, Z., and Tang, Z.: Atlas of woody plants in China: distribution and climate, Springer Science & Business Media, 2011.

Fielding, A. H. and Bell, J. F.: A review of methods for the assessment of prediction errors in conservation presence/absence models, Environ. Conserv., 24, 38–49, https://doi.org/10.1017/s0376892997000088, 1997.

Fisher, J. I., Mustard, J. F., and Vadeboncoeur, M. A.: Green leaf phenology at Landsat resolution: Scaling from the field to the satellite, Remote Sens. Environ., 100, 265–279, https://doi.org/10.1016/j.rse.2005.10.022, 2006.

Fitchett, J. M., Grab, S. W., and Thompson, D. I.: Plant phenology and climate change: Progress in methodological approaches and application, Prog. Phys. Geogr., 39, 460–482, https://doi.org/10.1177/0309133315578940, 2015.

Friedl, M. and Sulla-Menashe, D.: MODIS/Terra+Aqua Land Cover Type Yearly L3 Global 500m SIN Grid V061, NASA EOSDIS Land Processes DAAC, https://doi.org/10.5067/MODIS/MCD12Q1.061, 2022.

Fu, Y., Li, X., Zhou, X., Geng, X., Guo, Y., and Zhang, Y.: Progress in plant phenology modeling under global climate change, Sci. China Earth Sci., 63, 1237–1247, https://doi.org/10.1007/s11430-019-9622-2, 2020.

Fu, Y. H., Zhao, H., Piao, S., Peaucelle, M., Peng, S., Zhou, G., Ciais, P., Huang, M., Menzel, A., Peñuelas, J., and others: Declining global warming effects on the phenology of spring leaf unfolding, Nature, 526, 104–107, https://doi.org/10.1038/nature15402, 2015.

Fu, Y. H., Piao, S., Delpierre, N., Hao, F., Hänninen, H., Liu, Y., Sun, W., Janssens, I. A., and Campioli, M.: Larger temperature response of autumn leaf senescence than spring leaf-out phenology, Global Change Biol., 24, 2159–2168, https://doi.org/10.1111/gcb.14021, 2018.

GBIF: GBIF Occurrence Download, accessed on 2022-08-12, https://doi.org/10.15468/dl.7dwjev, 2022.

Ge, Q., Wang, H., and Dai, J.: Simulating changes in the leaf unfolding time of 20 plant species in China over the twenty-first century, Int. J. Biometeorol., 58, 473–484, https://doi.org/10.1007/s00484-013-0671-x, 2014.

Ge, Q., Wang, H., Rutishauser, T., and Dai, J.: Phenological response to climate change in China: a meta-analysis, Global Change Biol., 21, 265–274, https://doi.org/10.1111/gcb.12648, 2015.

Gill, A. L., Gallinat, A. S., Sanders-DeMott, R., Rigden, A. J., Short Gianotti, D. J., Mantooth, J. A., and Templer, P. H.: Changes in autumn senescence in northern hemisphere deciduous trees: a meta-analysis of autumn phenology studies, Ann Bot, 116, 875–888, https://doi.org/10.1093/aob/mcv055, 2015.

Hufkens, K., Basler, D., Milliman, T., Melaas, E. K., and Richardson, A. D.: An integrated phenology modelling framework in R, Methods Ecol. Evol., 9, 1276–1285, https://doi.org/10.1111/2041-210x.12970, 2018.

Izquierdo-Verdiguier, E., Zurita-Milla, R., Ault, T. R., and Schwartz, M. D.: Development and analysis of spring plant phenology products: 36 years of 1-km grids over the conterminous US, Agric. For. Meteorol., 262, 34–41, https://doi.org/10.1016/j.agrformet.2018.06.028, 2018.

Jeong, S.-J. and Medvigy, D.: Macroscale prediction of autumn leaf coloration throughout the continental United States, Global Ecol. Biogeogr., 23, 1245–1254, https://doi.org/10.1111/geb.12206, 2014.

Keenan, T. F., Gray, J., Friedl, M. A., Toomey, M., Bohrer, G., Hollinger, D. Y., Munger, J. W., O'Keefe, J., Schmid, H. P., Wing, I. S., and others: Net carbon uptake has increased through warming-induced changes in temperate forest phenology, Nat. Clim. Change, 4, 598–604, https://doi.org/10.1038/nclimate2253, 2014.

Kowalski, K., Senf, C., Hostert, P., and Pflugmacher, D.: Characterizing spring phenology of temperate broadleaf forests using Landsat and Sentinel-2 time series, Int. J. Appl. Earth Obs. Geoinf., 92, 102172, https://doi.org/10.1016/j.jag.2020.102172, 2020.

Lang, W., Chen, X., Qian, S., Liu, G., and Piao, S.: A new process-based model for predicting autumn phenology: how is leaf senescence controlled by photoperiod and temperature coupling?, Agric. For. Meteorol., 268, 124–135, https://doi.org/10.1016/j.agrformet.2019.01.006, 2019.

Li, X., Zhou, Y., Meng, L., Asrar, G. R., Lu, C., and Wu, Q.: A dataset of 30 m annual vegetation phenology indicators (1985–2015) in urban areas of the conterminous United States, Earth Syst. Sci. Data, 11, 881–894, https://doi.org/10.5194/essd-11-881-2019, 2019.

Liang, L., Schwartz, M. D., and Fei, S.: Validating satellite phenology through intensive ground observation and landscape scaling in a mixed seasonal forest, Remote Sens. Environ., 115, 143–157, https://doi.org/10.1016/j.rse.2010.08.013, 2011.

Lieth, H.: Purposes of a phenology book, in: Phenology and Seasonality Modeling, edited by: Lieth, H., Springer, Berlin, Heidelberg, 3–19, https://doi.org/10.1007/978-3-642-51863-8_1, 1974.

Liu, H., Gong, P., Wang, J., Clinton, N., Bai, Y., and Liang, S.: Annual dynamics of global land cover and its long-term changes from 1982 to 2015, Earth Syst. Sci. Data, 12, 1217–1243, https://doi.org/10.5194/essd-12-1217-2020, 2020.

Liu, Q., Fu, Y. H., Zhu, Z., Liu, Y., Liu, Z., Huang, M., Janssens, I. A., and Piao, S.: Delayed autumn phenology in the Northern Hemisphere is related to change in both climate and spring phenology, Global Change Biol., 22, 3702–3711, https://doi.org/10.1111/gcb.13311, 2016a.

Liu, Y., Wu, C., Peng, D., Xu, S., Gonsamo, A., Jassal, R. S., Arain, M. A., Lu, L., Fang, B., and Chen, J. M.: Improved modeling of land surface phenology using MODIS land surface reflectance and temperature at evergreen needleleaf forests of central North America, Remote Sens. Environ., 176, 152–162, https://doi.org/10.1016/j.rse.2016.01.021, 2016b.

Melaas, E. K., Sulla-Menashe, D., Gray, J. M., Black, T. A., Morin, T. H., Richardson, A. D., and Friedl, M. A.: Multisite analysis of land surface phenology in North American temperate and boreal deciduous forests from Landsat, Remote Sens. Environ., 186, 452–464, https://doi.org/10.1016/j.rse.2016.09.014, 2016.

Menzel, A.: Phenology: its importance to the global change community, Clim. Change, 54, 379, https://doi.org/10.1023/A:1016125215496, 2002.

Menzel, A., Yuan, Y., Matiu, M., Sparks, T., Scheifinger, H., Gehrig, R., and Estrella, N.: Climate change fingerprints in recent European plant phenology, Global Change Biol., 26, 2599–2612, https://doi.org/10.1111/gcb.15000, 2020.

Misra, G., Cawkwell, F., and Wingler, A.: Status of phenological research using Sentinel-2 data: A review, Remote Sens., 12, 2760, https://doi.org/10.3390/rs12172760, 2020.

Muñoz Sabater, J.: ERA5-Land hourly data from 1981 to present, Copernicus Climate Change Service (C3S) Climate Data Store (CDS), 2019.

Muñoz Sabater, J.: ERA5-Land hourly data from 1950 to 1980, Copernicus Climate Change Service (C3S) Climate Data Store (CDS), 2021.

Muñoz-Sabater, J., Dutra, E., Agustí-Panareda, A., Albergel, C., Arduini, G., Balsamo, G., Boussetta, S., Choulga, M., Harrigan, S., Hersbach, H., and others: ERA5-Land: A state-of-the-art global reanalysis dataset for land applications, Earth Syst. Sci. Data, 13, 4349–4383, https://doi.org/10.5194/essd-13-4349-2021, 2021.

Park, D. S., Newman, E. A., and Breckheimer, I. K.: Scale gaps in landscape phenology: challenges and opportunities, Trends Ecol. Evol., 36, 709–721, https://doi.org/10.1016/j.tree.2021.04.008, 2021.

Peng, D., Wu, C., Li, C., Zhang, X., Liu, Z., Ye, H., Luo, S., Liu, X., Hu, Y., and Fang, B.: Spring green-up phenology products derived from MODIS NDVI and EVI: Intercomparison, interpretation and validation using National Phenology Network and AmeriFlux observations, Ecol. Indic., 77, 323–336, https://doi.org/10.1016/j.ecolind.2017.02.024, 2017.

Phillips, S. J., Anderson, R. P., and Schapire, R. E.: Maximum entropy modeling of species geographic distributions, Ecol. Modell., 190, 231–259, https://doi.org/10.1016/j.ecolmodel.2005.03.026, 2006.

Piao, S., Liu, Q., Chen, A., Janssens, I. A., Fu, Y., Dai, J., Liu, L., Lian, X., Shen, M., and Zhu, X.: Plant phenology and global climate change: Current progresses and challenges, Glob Chang Biol, 25, 1922–1940, https://doi.org/10.1111/gcb.14619, 2019.

Polgar, C. A. and Primack, R. B.: Leaf-out phenology of temperate woody plants: from trees to ecosystems, New Phytol., 191, 926–941, https://doi.org/10.1111/j.1469-8137.2011.03803.x, 2011.

Pukelsheim, F.: The three sigma rule, Am. Stat., 48, 88–91, https://doi.org/10.2307/2684253, 1994.

Richardson, A. D., Keenan, T. F., Migliavacca, M., Ryu, Y., Sonnentag, O., and Toomey, M.: Climate change, phenology, and phenological control of vegetation feedbacks to the climate system, Agric. For. Meteorol., 169, 156–173, https://doi.org/10.1016/j.agrformet.2012.09.012, 2013.

549 Richardson, A. D., Hufkens, K., Milliman, T., Aubrecht, D. M., Chen, M., Gray, J. M., Johnston, M. R., Keenan, T. F.,
550 Klosterman, S. T., Kosmala, M., and others: Tracking vegetation phenology across diverse North American biomes
551 using PhenoCam imagery, Sci. Data, 5, 1–24, https://doi.org/10.1038/sdata.2018.28, 2018.
552 Rodriguez-Galiano, V., Dash, J., and Atkinson, P. M.: Intercomparison of satellite sensor land surface phenology and ground
553 phenology in Europe, Geophys. Res. Lett., 42, 2253–2260, https://doi.org/10.1002/2015gl063586, 2015.
554 Sagarin, R. D. and Gaines, S. D.: The 'abundant centre' distribution: to what extent is it a biogeographical rule?, Ecol. Lett.,
555 5, 137–147, https://doi.org/10.1046/j.1461-0248.2002.00297.x, 2002.
556 Schwartz, M. D.: Phenology: an integrative environmental science, Springer, 2003.
557 Studer, S., Stöckli, R., Appenzeller, C., and Vidale, P. L.: A comparative study of satellite and ground-based phenology, Int.
558 J. Biometeorol., 51, 405–414, https://doi.org/10.1007/s00484-006-0080-5, 2007.
559 Tang, J., Körner, C., Muraoka, H., Piao, S., Shen, M., Thackeray, S. J., and Yang, X.: Emerging opportunities and
560 challenges in phenology: a review, Ecosphere, 7, e01436, https://doi.org/10.1002/ecs2.1436, 2016.
561 Tao, Z., Wang, H., Dai, J., Alatalo, J., and Ge, Q.: Modeling spatiotemporal variations in leaf coloring date of three tree
562 species across China, Agric. For. Meteorol., 249, 310–318, https://doi.org/10.1016/j.agrformet.2017.10.034, 2018.
563 Templ, B., Koch, E., Bolmgren, K., Ungersböck, M., Paul, A., Scheifinger, H., Rutishauser, T., Busto, M., Chmielewski, F.-
564 M., Hájková, L., and others: Pan European Phenological database (PEP725): a single point of access for European data,
565 Int. J. Biometeorol., 62, 1109–1113, https://doi.org/10.1007/s00484-018-1512-8, 2018.
566 Tian, F., Cai, Z., Jin, H., Hufkens, K., Scheifinger, H., Tagesson, T., Smets, B., Van Hoolst, R., Bonte, K., Ivits, E., and
567 others: Calibrating vegetation phenology from Sentinel-2 using eddy covariance, PhenoCam, and PEP725 networks
568 across Europe, Remote Sens. Environ., 260, 112456, https://doi.org/10.1016/j.rse.2021.112456, 2021.
569 Wang, H., Dai, J., and Ge, Q.: The spatiotemporal characteristics of spring phenophase changes of Fraxinus chinensis in
570 China from 1952 to 2007, Sci. China Earth Sci., 55, 991–1000, https://doi.org/10.1007/s11430-011-4349-0, 2012.
571 Wang, H., Wu, C., Ciais, P., Peñuelas, J., Dai, J., Fu, Y., and Ge, Q.: Overestimation of the effect of climatic warming on
572 spring phenology due to misrepresentation of chilling, Nat. Commun., 11, 4945, https://doi.org/10.1038/s41467-020-
573 18743-8, 2020.
574 Wu, C., Hou, X., Peng, D., Gonsamo, A., and Xu, S.: Land surface phenology of China's temperate ecosystems over 1999–
575 2013: Spatial–temporal patterns, interaction effects, covariation with climate and implications for productivity,
576 Agricultural and Forest Meteorology, 216, 177–187, https://doi.org/10.1016/j.agrformet.2015.10.015, 2016.
577 Wu, C., Wang, X., Wang, H., Ciais, P., Peñuelas, J., Myneni, R. B., Desai, A. R., Gough, C. M., Gonsamo, A., Black, A. T.,
578 and others: Contrasting responses of autumn-leaf senescence to daytime and night-time warming, Nat. Clim. Change, 8,
579 1092–1096, https://doi.org/10.1038/s41558-018-0346-z, 2018.
580 Wu, W., Sun, Y., Xiao, K., and Xin, Q.: Development of a global annual land surface phenology dataset for 1982–2018 from
581 the AVHRR data by implementing multiple phenology retrieving methods, Int. J. Appl. Earth Obs. Geoinf., 103,
582 102487, https://doi.org/10.1016/j.jag.2021.102487, 2021a.

583 Wu, Z., Chen, S., De Boeck, H. J., Stenseth, N. C., Tang, J., Vitasse, Y., Wang, S., Zohner, C., and Fu, Y. H.: Atmospheric
584 brightening counteracts warming-induced delays in autumn phenology of temperate trees in Europe, Global Ecol.
585 Biogeogr., 30, 2477–2487, https://doi.org/10.1111/geb.13404, 2021b.
586 Ye, Y., Zhang, X., Shen, Y., Wang, J., Crimmins, T., and Scheifinger, H.: An optimal method for validating satellite-derived
587 land surface phenology using in-situ observations from national phenology networks, ISPRS J. Photogramm. Remote
588 Sens., 194, 74–90, https://doi.org/10.1016/j.isprsjprs.2022.09.018, 2022.
589 Zani, D., Crowther, T. W., Mo, L., Renner, S. S., and Zohner, C. M.: Increased growing-season productivity drives earlier
590 autumn leaf senescence in temperate trees, Science, 370, 1066–1071, https://doi.org/10.1126/science.abd8911, 2020.
591 Zhang, X., Wang, J., Gao, F., Liu, Y., Schaaf, C., Friedl, M., Yu, Y., Jayavelu, S., Gray, J., Liu, L., and others: Exploration
592 of scaling effects on coarse resolution land surface phenology, Remote Sens. Environ., 190, 318–330,
593 https://doi.org/10.1016/j.rse.2017.01.001, 2017.
594 Zhang, X., Friedl, M., and Henebry, G.: VIIRS/NPP Land Cover Dynamics Yearly L3 Global 0.05 Deg CMG V001, NASA
595 EOSDIS Land Processes DAAC, accessed on 2022-08-11, https://doi.org/10.5067/VIIRS/VNP22C2.001, 2020.
596 Zhu, M., Dai J.: Species phenology and ground phenology maps over China from 1951-2020, Science Data Bank [data set],
597 https://doi.org/10.57760/sciencedb.07995. DOI:10.57760/sciencedb.07995, 2023.